AIAA'85

AIAA-85-0392

THE DETONABILITY OF RDX DUST IN AIR-OXYGEN MIXTURES

F. P. Lee, C. W. Kauffman, M. Sichel and J. A. Nicholls
Department of Aerospace Engineering,
The University of Michigan, Ann Arbor 48109-2140

AIAA 23rd Aerospace Sciences Meeting

January 14-17, 1985/Reno, Nevada

THE DETONABILITY OF RDX DUST IN AIR-OXYGEN MIXTURES

F. P. Lee, C. W. Kauffman, M. Sichel and J. A. Nicholls
Department of Aerospace Engineering
The University of Michigan
Ann Arbor, MI 48109-2140

Abstract

A combined experimental and theoretical study was conducted to determine the detonability characteristics of high explosive RDX dust dispersed in air. Towards this end, a special "shock tube" was constructed in which the dust was transported through the tube by a gas flow. Detonation of high pressure gases in the driver served to transmit a strong blast wave into the dust mixture. The resultant wave was monitored by pressure switches, pressure transducers, a photocell, and streak photography. Within the limits of the facility detonation was realized for dust with the larger of the particles (37 μ) tested in oxygen enriched air (12% O_2 + 88% air by volume) and with ammonium perchlorate added to the dust mixture as additional oxidizer (17% AP + 83% RDX by mass) in air. However, under the same conditions, the finer dust with the smaller particles (2 μ) could not be detonated.

A theoretical model was developed to explain the effect of particle size on the detonability of dust oxidizer mixtures. In this model an unsteady particle heat transfer equation with an Arrhenius type of reactive source term was coupled with the flow conservation equations. The thermal effect due to the presence of particles on the flow prior to ignition were calculated for various particle sizes and loading ratios. It was shown that a large concentration of very fine dust mixed with the gaseous oxidizer would cool down the gas behind the incident shock wave sufficiently to deter the ignition of the particles. This provides an explanation for why the finer dust failed to detonate.

Introduction

Safety considerations make it important to establish the detonability characteristics of mixtures of dust with air or air enriched with oxygen. RDX dust is of particular interest because it is a commonly used explosive, and because as an explosive, it contains its own oxidizer. For this reason, detonations were induced in RDX dust-air-oxygen mixtures using a horizontal shock tube with an explosive driver. RDX dusts with 2 μm diameter particles and with 37 μm particles were investigated. Neither of these dusts would detonate in air, but detonations in the coarse dust were observed in a 12% oxygen/88% air mixture. Remarkably, and contrary to intuition, it was impossible to detonate the fine dust in this mixture. Theoretical analysis shows that this behavior is a consequence of the interaction between the dust particles and the gas in the two phase flow within the induction zone.

The experimental apparatus is first described below followed by a presentation of experimental results. The analysis of the two phase flow within the induction zone is then described and the results of the analysis are used to show how the interaction between the dust particles and the gas flow provides an explanation for the failure of detonation in the fine grained dust.

Experimental Arrangement

Experiments were conducted in a horizontal shock tube (shown in Fig. 1a) with a 7.3 cm diameter driver section 37 cm long and a 3.8 cm × 6.4 cm rectangular driven section 7 m long. A 30 cm long transition section was used to connect the circular driver to the rectangular driven section. A feeder to introduce the dust was mounted on top of the transition section. The dust feeder (shown in Figs. 1b and 1c) consisted of a piston in a plastic cartridge, a pulling motor, and several air feeding jets. During operation, the motor pulled the piston which in turn pushed a predetermined quantity of RDX dust loaded in the cartridge into the path of the air jets which blew the dust into the shock tube. The dust entering the shock tube was then conveyed through the tube by gaseous oxidizer from two jets mounted on both sides of the transition section. The dust concentration in the flow mixture was determined by the mass feeding rate of dust (gm/sec) and the volumetric flow rate of the conveying gas (m^3/sec). Detonation of a $2H_2 + O_2 +$ He mixture in the driver served as the initiator and caused a shock wave to be transmitted into the dust cloud in the driver section. The shock wave velocity was measured by six pressure switches, and the pressure by a four Kistler 603A pressure transducers. A photocell was located at the same position as No. 3 pressure transducer to measure the ignition delay. The shock wave and flow interaction were observed using streak Schlieren photography at the window section of the shock tube.

Experimental Results

RDX dusts with average particle diameters of 2μ and 37μ were tested in air, oxygen enriched air and nitrogen. Photomicrographs of the two dusts are shown in Fig. 2. The 2μ dust is very fine and tends to agglomerate as indicated in the photomicrograph. Therefore it was mixed with a small amount (2%) of inert amorphous fumed silica (SiO_2) dust to improve the dispersion characteristics of the dust along the tube. Streak photographs of the induction zone indicated that this technique successfully eliminated the agglomeration of the fine 2μ dust. The chemical and physical properties of RDX are presented in Table II below. Additional experiments were also made using ammonium perchlorate (AP) dust mixed with RDX as a supplementary solid oxidizer.

The velocity variations of the shock wave transmitted from the driver and the character of the pressure and photocell traces behind the shock were used to distinguish detonating from nondetonating mixtures. The wave velocity did not attenuate in the case of detonation and there was a large pressure rise followed by a decaying region behind the wave. The ignition delay, as determined from the photocell and pressure traces, was relatively short. In the nondetonating case, there was significant shock decay, a relatively low pressure rise and a long ignition delay period. The pressure and

Table I

Detonation Results for RDX Dust (37μ)

Mixture	Dust Concentration (gm/m^3)	Loading Ratio	Equivalence Ratio	Detonation Mach No.	Maximum Detonation Pressure (atm)
RDX in air/O_2 (88/17)	1300	0.99	0.86	5.1	32
RDX/AP (83/17) in air	1340	1.03	0.84	4.9	32
RDX/AP (83/17) in air	1500	1.15	0.88	5.0	34

photocell traces shown in Figs. 3a and 3b illustrate these differences.

Within the limits of the facility, the experimental results showed that RDX dust in air would not detonate. However, detonation was realized with the coarser dust in oxygen enriched air (12% oxygen + 88% air), and also in an AP-RDX dust mixture (17% AP/83% RDX) in air. The equivalence ratios used were slightly less than one and the loading ratio, i.e. the ratio of fuel to air mass were approximately one. The results for detonating runs are listed in Table I.

However, under the same operating conditions the finer dust with the 2μ particles did not detonate. The measured ignition delay shown in Fig. 3c for the nondetonating fine dust was about six times that of the detonating coarse dust shown in Fig. 3a, even though the combustion time of the fine dust is about one-quarter that of coarse dust.

These results are contrary to intuition, which would suggest that the finer dust would be more detonable. As shown in the analysis below, rapid absorption of heat by the finer dust can reduce the temperature and thereby greatly increase the ignition delay. This effect provides a possible explanation for the inability to detonate the fine dust.

Theoretical Analysis

A theoretical model was developed to deal with the interaction between the particles and the gas in the two phase flow behind the shock wave. This flow is shown schematically in Fig. 4 in coordinates which are fixed to the shock so that the shock becomes stationary while the wall moves with the undisturbed velocity u_o. Immediately behind the shock the velocity of the dust particles relative to the gas, i.e., $u_p - u$, may be supersonic. Thus bow shocks may stand ahead of the particles initially as shown in the schematic sketch in Fig. 4.

The equations for the conservation of mass, momentum, and energy are:

$$\rho u + \sigma_p u_p = \rho_o u_o + \sigma_{p_o} u_o \qquad (1)$$

$$\rho u^2 + \sigma_p u_p^2 + P + W_L = \rho_o u_o^2 + \sigma_{p_o} u_o^2 + P_o \qquad (2)$$

$$\rho u\left(\frac{u^2}{2} + h\right) + \sigma_p u_p\left(\frac{u_p^2}{2} + \bar{h}_p + Q\right) + Q_W - Q_S = H_o \qquad (3)$$

All symbols are defined in the nomenclature. These equations are discussed in detail by Rudinger[1], but have been supplemented by the addition of wall losses and the heat of combustion of the fuel particles. The momentum loss W_L, wall heat transfer Q_W, and viscous dissipation Q_S are evaluated from the expression given by Ragland, et al.[2]

$$W_L = \frac{4}{D_h}\int_o^x \tau_w dx \cong \frac{4x}{D_h} C_f \frac{\rho(u_o-u)^2}{2}$$

$$Q_W = \frac{4}{D_h}\int_o^x q_w dx \cong \frac{4x}{D_h}\left(\frac{C_f}{2}\right)\rho(u_o-u)\left[h + \frac{(u_o-u)^2}{2} - h_w\right]$$

$$Q_S = \frac{4}{D_h}\int_o^x \tau_w u_o dx \cong \frac{4x}{D_h}\left(\frac{C_f}{2}\right)\rho u_o (u_o-u)^2$$

where the mean friction coefficient C_f for the flow is taken as[2]

$$C_f = 0.074\,(Re)^{-1/5} = 0.074\left[\frac{\rho u x}{\mu}\right]^{-1/5}$$

The radiation has been approximated by assuming that the particles radiate to the wall as a grey body so that

$$Q_R = \frac{4}{D_h}\int_o^x q_r dx \cong 4\,\frac{x}{D_h}\,\varepsilon'\sigma' T^4$$

The radiative loss was found to be negligible even when the emissivity ε' is taken as unity. This result is probably a consequence of the short time available for radiation in the induction zone.

As written above, these equations treat the gas-particle mixture as a single fluid. The interaction between the particles and the gas is introduced through the trajectory equation:

$$\frac{4}{3}\pi R^3 \rho_p \frac{du_p}{dt} = \frac{1}{3} C_D \rho \pi R^2 (u-u_p)|u - u_p| \qquad (4)$$

which is needed to determine the particle velocity and accounts for the exchange of momentum between the gas and the particles. The thermal interaction between the gas and the particles, which is crucial in the analysis of the induction zone, is determined by the heat transfer between the gas and the particles. To simplify the thermal analysis, it has been assumed that the particles are spherical and that the temperature distribution within the particles is spherically symmetric. It has further been assumed that the dust cloud is monodisperse. If $T_f(t)$ is the recovery temperature based on the velocity of the gas relative to the particle, and

if $T(R,t)$ is the temperature at the particle surface, then the rate of change of the enthalpy H_p of each particle will be given by

$$\frac{dH_p}{dt} = 4\pi R^2 h(t)[T_f(t) - T(R,t)] \quad (5)$$

where the particle enthalpy H_p can be expressed by

$$H_p = \int_0^R 4\pi r^2 C\, T(r)dr$$

and the average specific enthalpy of the particle, $\bar{h}_p$, is given by

$$\bar{h}_p = \frac{H_p}{m_p}$$

where $m_p = 4/3\pi R^3 \rho_p$ is the mass of each particle. The film conductance $h(t)$ depends on the velocity of the gas relative to the particles. In general, it also is necessary to introduce a reaction rate equation to account for the particle combustion and the rate of change of the particle mass flow density $\sigma_p u_p$; however, this term can be neglected in the induction zone preceding the start of combustion.

For the particle sizes considered here, previous studies of shock induced ignition indicate that ignition is governed by heterogeneous reaction at the particle surface, particularly since in the case shock ignition there appears to be insufficient time for the evolution of significant amounts of volatiles. Accepting surface reaction as the driving mechanism, ignition first occurs at the particle surface where the particle temperature has the highest value during heat up. Because of the large values of the Biot number, the temperature within the particle will not be uniform, and calculation of particle surface temperature requires solution of the heat conduction equation:

$$\frac{\partial T}{\partial t} = \frac{\alpha}{r^2}\frac{\partial}{\partial r}\left(r^2 \frac{\partial T}{\partial r}\right) + \frac{u'''(r,t)}{\rho_p C} \quad (6)$$

A source term $u'''(r,t)$ is included to account for the heat released by heterogeneous reaction both on the particle surface and in the porous interior of the particle. The boundary condition at the particle surface is governed by convective heat transfer from the surrounding gas and is given by:

$$K_p \frac{\partial T}{\partial r}\Big|_{r=R} = h(t)[T_f(t) - T(R,t)] \quad (7)$$

Evaluation of the reactive source term is a major source of uncertainty because of the lack of adequate chemical kinetic data for dusts. Assuming a first order reaction, as was also done by Ural, et al.[3], and Sichel, et al.[4]. This term will be given by:

$$u''' = Q\rho_p S_i p_{O_2} \exp(-E/\bar{R}T) \quad (8)$$

The values of the parameters used in the computations are listed in Table II below. Due to the lack of kinetic data available for RDX, some of the parameters used in (8) were determined by comparing the results of the present theory to ignition delay data.

It also is necessary to choose suitable values for the drag coefficient C_D in (4) and for the film conductance $h(t)$ in (5) and (7). The velocity relative to the particles varies from supersonic values to values in the Stokes drag regime. To cover this wide range, the empirical expressions for C_D presented by Walsh[5] were used in the computations, and it turns out that C_D varies significantly during particle acceleration. The Nusselt No. and hence $h(t)$ also varies over a wide range during particle acceleration, and hence the empirical expression for h given by Fox[6] was used to evaluate $h(t)$. According to Fox

$$Nu = 2Rh/K_{pr} = 2e^{-M}/(1 + 17M/Re) + 0.459P_r^{0.33} \cdot Re^{0.55}(1.0 + 0.5e^{-17M/Re})/1.5 \quad (9)$$

The structure of the induction zone and the ignition delay time were determined by numerically solving Eqs. (1) - (9). The ignition delay was taken as the time between shock passage and particle surface temperature runaway. Ignition delays were calculated over a wide range of particle loading and particle size.

The detailed gas and particle surface temperature variations are shown in Figs. 5a and 5b for 2μ and 37μ particles for a loading ratio, $(\sigma_p/\rho)_o$ upstream of the shock wave, of 1.0. In the case of the 2μ particles, both the gas and particle surface temperature initially rise very rapidly. Then, because of the greater surface are of the smaller particles, both the gas and particle surface temperatures drop to a lower steady value until ignition. On the other hand, in the case of the larger 37μ particles, the surface temperature rises steadily until ignition occurs. As a consequence, contrary to intuition, the ignition delay of 52μ sec of the 2μ dust is four times the 13μ sec delay of the coarser 37μ dust.

This behavior is also mirrored by the interior temperature distribution of the 2μ and 37μ particles which is shown in Figs. 6a and 6b at time increments of 1μ sec. In the case of the 2μ particles, the surface temperature increases rapidly after which it drops while the temperature in the interior of the particle becomes almost uniform. These small particles are thus very effective in absorbing heat from the surrounding gas stream, and this accounts for the drop in both gas and particle temperature shown in Fig. 5. In the case of the 37μ particles, the heated region is confined almost entirely to the vicinity of the particle surface and the surface temperature increases continuously.

The influence of the particle interaction on the gas temperature and ignition delay depends on both the loading ratio and the particle size as illustrated in Fig. 7. This figure shows the variation of the ignition delay with particle size for different values of particle loading as calculated using the theory described above. The ignition delay always decreases with decreasing particle size for small loading ratios when the particle/gas interaction is weak. However, for loading ratios of O(1), the ignition delay increases drastically when the particle diameter drops below about 6μ.

Discussion and Conclusions

Experiments have demonstrated that mixtures of 2μ and 37μ RDX dust with air could not be made to detonate. It was possible to induce detonations in the 37μ dust in an 88% air/12% O_2 mixture and in an

83% RDX/17% AP mixture in air. However, 2μ RDX dust under the same conditions could not be detonated in the oxygen enriched air.

Theoretical analysis of the two phase flow in the induction zone showed that this effect could be explained by the rapid absorption of heat by the smaller particles, which resulted in a reduced gas temperature and a corresponding increase in the ignition delay. Other explanations are of course also possible. Thus failure to detonate might be caused by the agglomeration of the smaller particles. However, streak photographs indicated that agglomeration was not a problem for the finer dust. Since RDX is an explosive, another explanation is that the smaller particles were less than the critical explosion diameter, while the larger particles acted like explosive pellets. However, increased heat absorption by the smaller particles appears as the most convincing explanation to the authors.

Perhaps the most important conclusion is that in any realistic analysis of the induction zone of dust detonations, it is absolutely essential to take the effects of two phase flow into account.

Table II

Thermal and Chemical Properties of RDX

Density (gm/cm^3)	$1.82^{(1)}$
Thermal conductivity (cal/cm-sec-°C)	6.98×10^{-4} (1)
Specific heat (cal/gm-°C)	$0.45^{(1)}$
Internal surface area (cm^2/gm)	8×10^6
Activation energy (K cal/gm-mole)	$17.5^{(2)}$
Pre-exponential Factor (gm/cm^2-sec-atm)	80

1 Ref. 7

2 Ref. 4

Acknowledgment

The authors would like to express their appreciation for support for the work reported here by the Air Force Office of Scientific Research under AFOSR Gratn No. 79-0093.

References

1. Rudinger, G., "Relaxation in Gas Particle Flow," Non-Equilibrium Flows, Marcel Dekker (1970).

2. Ragland, K. W., Dabora, E. K., and Nicholls, J. A., "Observed Structure of Spray Detonations," Physics of Fluids 11, 2377 (1968).

3. Ural, E. A., Sichel, M., and Kauffman, C. W., "Shock Wave Ignition of Pulverized Coal," 13th International Symposium on Shock Tubes and Waves.

4. Sichel, M., Back, S. W., Maker, B., Kauffman, C. W., Nicholls, J. A., and Wolanski, P., "The Shock Wave Ignition of Dusts," 22nd AIAA Space Science Meeting, Propellant and Combustion, January 1983.

5. Walsh, M. J., "Drag Coefficient Equations for Small Particles in High Speed Flow," AIAA J., 13, 11, 1526 (1975).

6. Fox, T. W., Rackett, C. W., and Nicholls, J.A. "Shock Wave Ignition of Magnesium Powder," 11th Int'l Symp. on Shock Tubes and Waves.

7. Engineering Design Handbook, Explosive Series, Properties of Explosives of Military Interest, U.S. Army Material Command, January 1971.

Nomenclature

A	Pre-exponential factor
C	Specific heat of particle
C_D	Drag coefficient
C_f	Mean friction coefficient
D_h	Hydraulic diameter of tube
E	Activation energy
h	Gas enthalpy
H_p	Enthalpy of individual particle
$\bar{h}_p$	Average specific enthalpy of particle
$h(t)$	Film conductance
K_p	Thermal conductivity of particle
K_{p_r}	Thermal conductivity of particle at recovery temperature
M	Mach number
P	Gas pressure
P_{O_2}	Oxygen partial pressure
Pr	Prandtl number
Q	Heat of combustion per unit particle mass
Q_R	Radiative heat transfer on the wall
Q_S	Viscous work done by wall on fluid per unit area
Q_W	Convective hat flux to the wall
R	Particle radius
r	Radius
$\bar{R}$	Gas constant
Re	Reynolds number
S_i	Internal surface
t	Time
T	Temperature
T_f	Recovery temperature
τ_w	Viscous force on the wall
u	Gas velocity
u_o	Shock wave velocity relative to the wall
u_p	Particle velocity
$\dot{w}'''$	Volumetric heating rate within particle
W_L	Fluid momentum loss due to wall friction
α	Thermal diffusivity of particle
ρ	Gas density
ρ_p	Density of particle material
σ_p	Particle mass per unit mixture volume
μ	Viscosity of gas
h_w	Enthalpy of gas at the wall

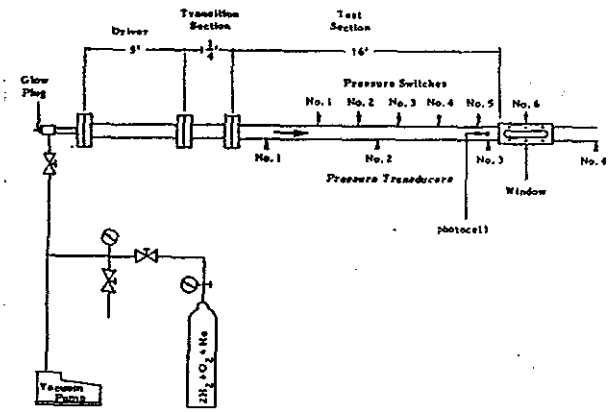

Figure 1a. Schematic of experimental setup.

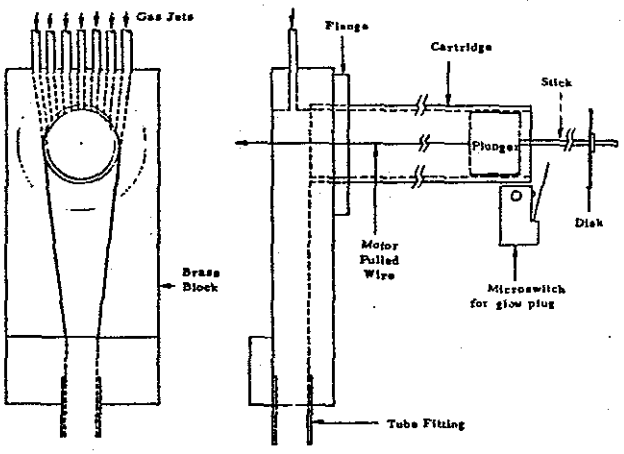

Figure 1b. Schematic of dust feeder.

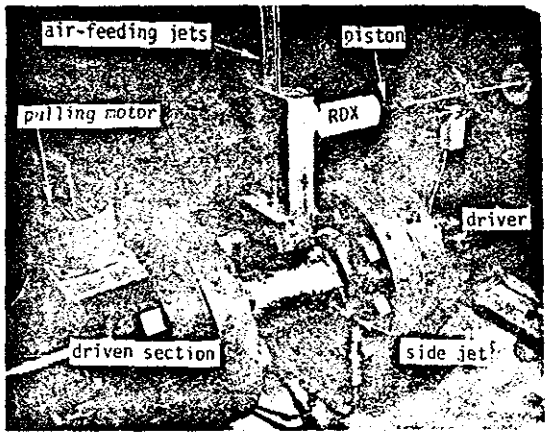

Figure 1c. Transition section and dust feeder.

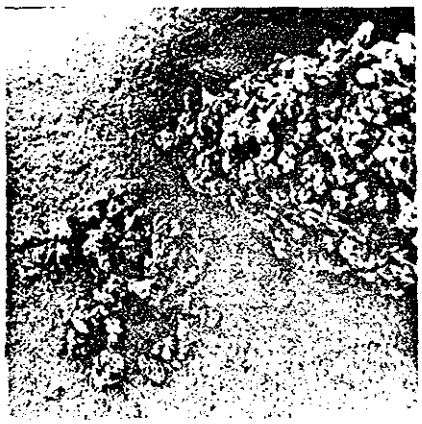

Figure 2. Photomicrographs of RDX, 100 X.

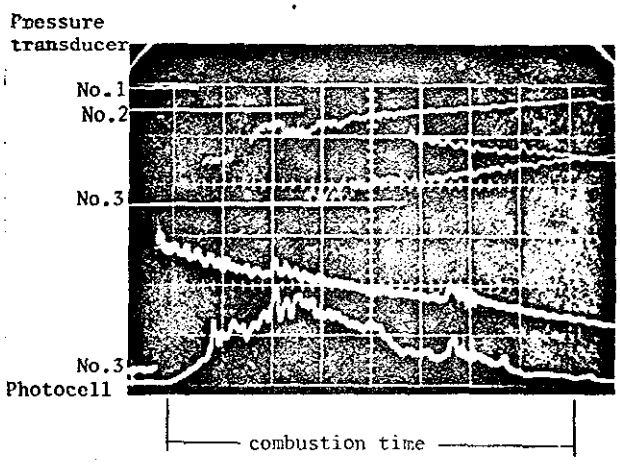

Figure 3a. RDX (37um) + air/O_2 (88/12), 1300gm/m^3, .5 msec/div.

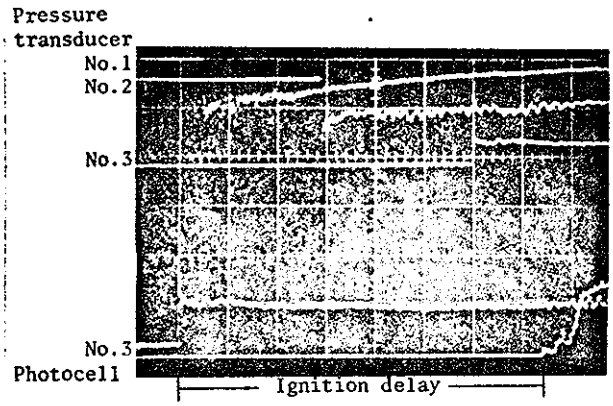

Figure 3b. RDX (37μm) + N_2, 1300 gm/m^3, .5msec/div.

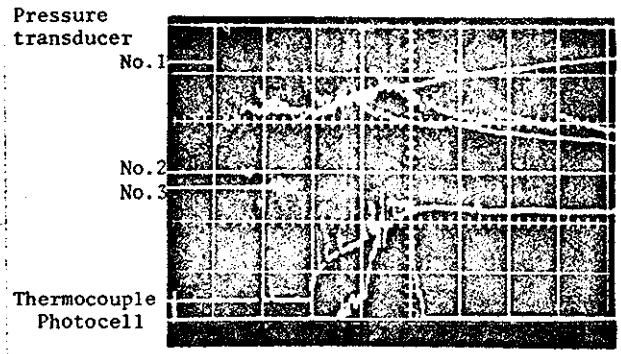

Figure 3c. RDX (2μm) + air/O_2 (88/12), 1300 gm/m^3, .5msec/div.

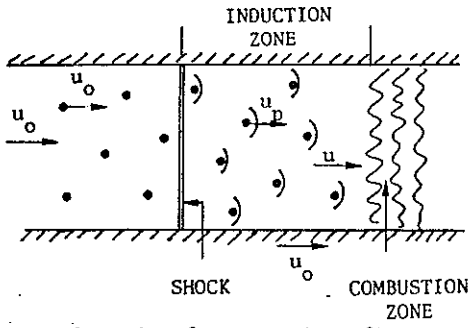

Figure 4. Schematic of gas-particle flow.

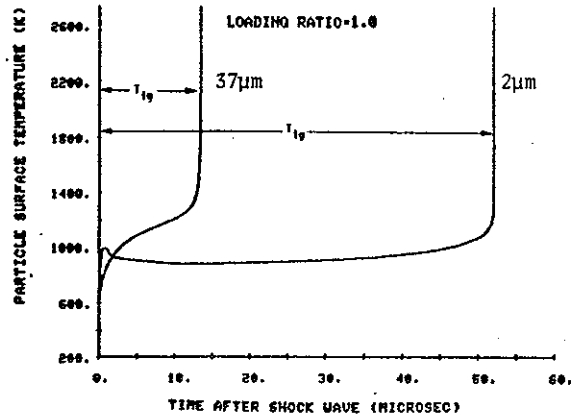

Figure 5a. Surface temperature histories of 2μm & 37μm RDX particles in air/O_2 (88/12) subject to shock wave of M=5.1.

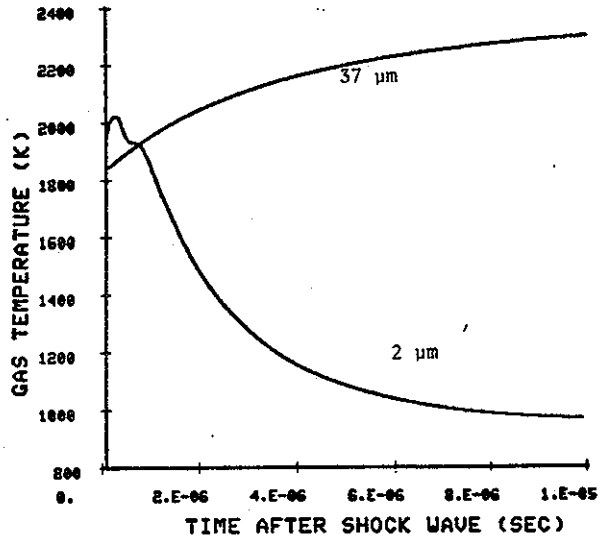

Figure 5b. Gas temperature histories. Same flow conditions as in Figue 5a.

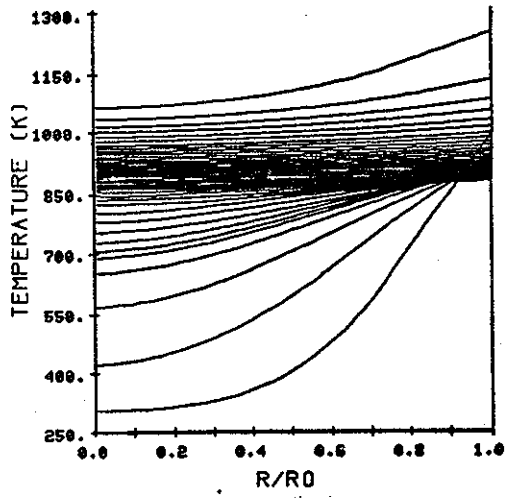

Figure 6a. Time histories of temperature distribution inside a 2μm RDX particle.

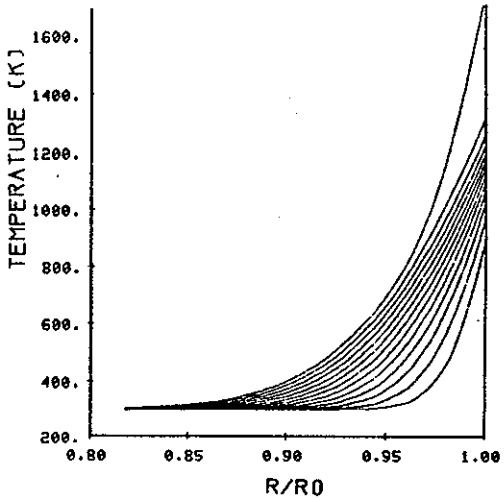

Figure 6b. Time histories of temperature distribution inside a 37μm RDX particle.

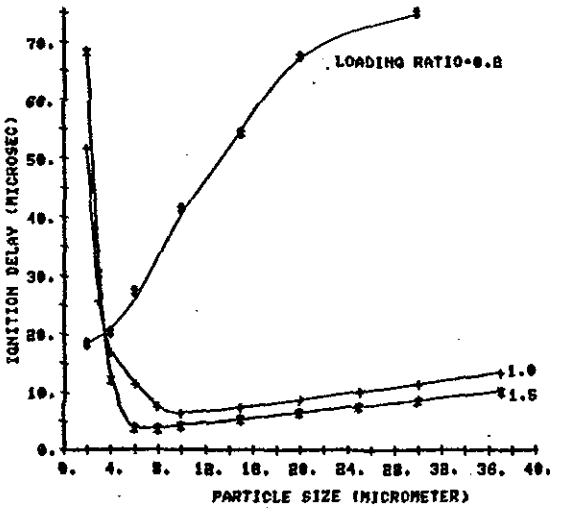

Figure 7. Ignition delay vs. particle size of RDX in air/O_2 (88/12) subject to shock wave of M=5.1.